4
Reciprocity between heavier baryons and meson condensation in dense matter

4.1 Introduction

Due to large densities reached in the core region of compact stars, new hadronic degrees of freedom are expected to nucleate in addition to the nucleons. One such possibility is the onset of hyperons, as initially suggested in ref.-Ambartsumyan and Saakyan [1960]. This occurs in the inner core of compact stars at about $(2-3)n_0$. Even though the presence of hyperons in compact stars may seem to be unavoidable, it leads to an incompatibility of the theory with the observations of massive pulsars mentioned above, as is evidenced by many studies which used either phenomenological [Glendenning, 1985; Weber and Weigel, 1989; Knorren et al., 1995; Balberg and Gal, 1997; Zhou et al., 2008] or microscopic [Schulze et al., 1995; Baldo et al., 1998; Vidaña et al., 2000; Sammarruca, 2009; Dapo et al., 2010] approaches. Specifically, hyperons lead to a softening of the EoS and imply a low value of the maximum mass of compact stars, below those observed. This problem is known as the "hyperon puzzle". The studies prior to the discovery of massive pulsars, the work during the last decade focused mainly on models which provide sufficient repulsion among the hadronic interactions which guarantees stiffer EoS and larger maximum masses of hypernuclear stars; these have been carried out mostly within the covariant density functional theory [Weissenborn et al., 2012; Bonanno and Sedrakian, 2012; Colucci and Sedrakian, 2013; van Dalen et al., 2014; Oertel et al., 2015; Chatterjee and Vidaña, 2016; Fortin et al., 2016; Chen et al., 2007; Drago et al., 2014; Cai et al., 2015; Zhu et al., 2016; Sahoo et al., 2018; Kolomeitsev et al., 2017; Li et al., 2018b; Li and Sedrakian, 2019; Ribes et al., 2019; Li et al., 2020]. But microscopic models have also been employed in works by Yamamoto et al. [2016]; Shahrbaf et al. [2020].

Another fascinating possibility of the onset of non-nucleonic degrees of freedom is the appearance of stable Δ-resonances in the matter. Whether Δ-resonances play any role in the NSs is still a matter of debate Li et al. [2018b]; Motta et al. [2020]. Early works Glendenning [1985]; Glendenning and Moszkowski [1991] indicated that the threshold density for the appearance of Δ-resonances could be as high as $(9-10)\ n_0$. More recent works [Li et al., 2018b; Drago et al., 2014; Drago et al., 2014; Cai et al., 2015] have shown that indeed these non-strange baryons may appear in nuclear matter at density in the range $(1-2)\ n_0$.

In this chapter, we explore the possibility of (anti)kaon condensation in β-equilibrated Δ-resonance admixed hypernuclear matter in the core region of compact stars within the frame-

work of RMF model. This chapter is arranged as follows. In sec.-4.2 we briefly describe the density-dependent RMF formalism and its extension to (anti)kaons condensation in Δ-resonances admixed hypernuclear matter followed by the coupling parameter estimations in sec.-4.3. Sec.-4.4 is devoted to numerical results and their discussions. The conclusions and future perspectives are given in Sec. 4.5. The work presented in this chapter is reported in ref.-Thapa et al. [2021].

4.2 Formalism

In this section, we extend the density-dependent RMF model to study the transition of matter from hadronic to (anti)kaon condensed phase in β-equilibrated Δ-resonance admixed hypernuclear matter. The matter composition is considered to be of the baryon octet ($b \equiv N, \Lambda, \Sigma, \Xi$), Δ-resonances ($\Delta \equiv \Delta^{++}, \Delta^{+}, \Delta^{0}, \Delta^{-}$), (anti)kaons ($\bar{K} \equiv K^{-}, \bar{K^0}$) alongside leptons ($l$) such as electrons and muons. The strong interactions between the baryons as well as the (anti)kaons are mediated similar as in nuclear matter case by the isoscalar-scalar σ, isoscalar-vector ω^{μ} and isovector-vector $\boldsymbol{\rho}^{\mu}$ meson fields. The additional hidden strangeness mesons (σ^{*}, ϕ^{μ}) are considered to mediate the hyperon-hyperon as well as (anti)kaon-hyperon interactions. It has been reported in ref.-Schaffner and Mishustin [1996] that the role of σ^{*} meson in hyperon-hyperon interaction is very weak. So, to have some insight in this aspect we have investigated the influence of additional strange isoscalar-scalar meson. The Lagrangian density consisting of the baryonic and leptonic parts is given by [Glendenning, 1996; Li et al., 2018b]

$$\begin{aligned}\mathcal{L} = &\sum_{b} \bar{\psi}_b(i\gamma_\mu D^{\mu}_{(b)} - m^{*}_{b})\psi_b + \sum_{\Delta} \bar{\psi}_{\Delta\nu}(i\gamma_\mu D^{\mu}_{(\Delta)} - m^{*}_{\Delta})\psi^{\nu}_{\Delta} + \sum_{l} \bar{\psi}_l(i\gamma_\mu \partial^{\mu} - m_l)\psi_l \\ &+ \frac{1}{2}(\partial_\mu \sigma \partial^{\mu}\sigma - m^2_{\sigma}\sigma^2) + \frac{1}{2}(\partial_\mu \sigma^{*} \partial^{\mu}\sigma^{*} - m^2_{\sigma^{*}}\sigma^{*2}) - \frac{1}{4}\omega_{\mu\nu}\omega^{\mu\nu} + \frac{1}{2}m^2_{\omega}\omega_{\mu}\omega^{\mu} \\ &- \frac{1}{4}\boldsymbol{\rho}_{\mu\nu}\cdot\boldsymbol{\rho}^{\mu\nu} + \frac{1}{2}m^2_{\rho}\boldsymbol{\rho}_{\mu}\cdot\boldsymbol{\rho}^{\mu} - \frac{1}{4}\phi_{\mu\nu}\phi^{\mu\nu} + \frac{1}{2}m^2_{\phi}\phi_{\mu}\phi^{\mu}\end{aligned} \tag{4.1}$$

where the fields ψ_b, ψ_l, ψ^{ν}_{Δ} correspond to the baryon octet, lepton (Dirac) and Δ-baryon (Rarita-Schwinger) fields. Unlike particles of the baryon octet and leptons (spin-1/2 particles), the Δ-resonances have spin of 3/2. So, to explain the dynamics of such particles Rarita-Schwinger equation [Rarita and Schwinger, 1941] has to be considered as Dirac equation fails to explain the same. m_b, m_d and m_l represent the bare masses of members of baryon octet, Δ-quartet and leptons respectively. The Lagrangian density for the (anti)kaons is described in sec.-3.2. The covariant derivative in eq.-(4.1) is defined as

$$D_{\mu(j)} = \partial_\mu + ig_{\omega j}\omega_\mu + ig_{\rho j}\boldsymbol{\tau}_j\cdot\boldsymbol{\rho}_\mu + ig_{\phi j}\phi_\mu \tag{4.2}$$

with j denoting the baryons (b, Δ). The density-dependent coupling constants are denoted by g_{pj} where 'p' index labels the mesons. The Dirac, Rarita-Schwinger effective baryon and (anti)kaon masses are given by

$$\begin{aligned} m^{*}_{b} &= m_b - g_{\sigma b}\sigma - g_{\sigma^{*} b}\sigma^{*}, \\ m^{*}_{\Delta} &= m_{\Delta} - g_{\sigma\Delta}\sigma, \\ m^{*}_{K} &= m_K - g_{\sigma K}\sigma - g_{\sigma^{*} K}\sigma^{*}. \end{aligned} \tag{4.3}$$

In the RMF approximation, the meson fields obtain expectation values are given by

$$\begin{aligned}
\sigma &= \sum_b \frac{1}{m_\sigma^2} g_{\sigma b} n_b^s + \sum_\Delta \frac{1}{m_\sigma^2} g_{\sigma\Delta} n_\Delta^s + \sum_{\bar{K}} \frac{1}{m_\sigma^2} g_{\sigma K} n_{\bar{K}}^s, \\
\sigma^* &= \sum_b \frac{1}{m_{\sigma^*}^2} g_{\sigma^* b} n_b^s + \sum_{\bar{K}} \frac{1}{m_{\sigma^*}^2} g_{\sigma^* K} n_{\bar{K}}^s, \\
\omega_0 &= \sum_b \frac{1}{m_\omega^2} g_{\omega b} n_b + \sum_\Delta \frac{1}{m_\omega^2} g_{\omega\Delta} n_\Delta - \sum_{\bar{K}} \frac{1}{m_\omega^2} g_{\omega K} n_{\bar{K}}, \\
\phi_0 &= \sum_b \frac{1}{m_\phi^2} g_{\phi b} n_b - \sum_{\bar{K}} \frac{1}{m_\phi^2} g_{\phi K} n_{\bar{K}}, \\
\rho_{03} &= \sum_b \frac{1}{m_\rho^2} g_{\rho b} \boldsymbol{\tau}_{b3} n_b + \sum_\Delta \frac{1}{m_\rho^2} g_{\rho\Delta} \boldsymbol{\tau}_{\Delta 3} n_\Delta + \sum_{\bar{K}} \frac{1}{m_\rho^2} g_{\rho K} \boldsymbol{\tau}_{\bar{K}3} n_{\bar{K}},
\end{aligned} \tag{4.4}$$

where $n^s = \langle\bar{\psi}\psi\rangle$ and $n = \langle\bar{\psi}\gamma^0\psi\rangle$ denote the scalar and vector (number) densities respectively as defined in chapters-2 and 3. The chemical potential of the j-th baryon is

$$\mu_j = \sqrt{p_{F_j}^2 + m_j^{*2}} + \Sigma_B, \tag{4.5}$$

where $\Sigma_B = \Sigma^0 + \Sigma^r$ denotes the vector self-energy with

$$\Sigma^0 = g_{\omega j}\omega_0 + g_{\phi j}\phi_0 + g_{\rho j}\boldsymbol{\tau}_{j3}\rho_{03}, \tag{4.6}$$

$$\Sigma^r = \sum_b \left[\frac{\partial g_{\omega b}}{\partial n}\omega_0 n_b - \frac{\partial g_{\sigma b}}{\partial n}\sigma n_b^s + \frac{\partial g_{\rho b}}{\partial n}\rho_{03}\boldsymbol{\tau}_{b3} n_b + \frac{\partial g_{\phi b}}{\partial n}\phi_0 n_b \right] + \sum_\Delta (\psi_b \longrightarrow \psi_\Delta^\nu). \tag{4.7}$$

Here, eq.-(4.7) is the rearrangement term which is required in case of density-dependent meson-baryon coupling models to maintain the thermodynamic consistency as already discussed in sec.-2.4.

As already discussed in chapter-2, to describe the dense NS matter the conditions which are necessary to maintain weak β-equilibrium between different particle species without strangeness being conserved are given by the relation [Glendenning, 1996]

$$\mu_j = \mu_n - q_j\mu_e \tag{4.8}$$

where q_j is the charge of the j-th baryon and which translates to

$$\begin{aligned}
\mu_e &= \mu_n - \mu_p = \mu_\mu, \\
\mu_{\Sigma^+} &= \mu_{\Delta^+} = \mu_p, \\
\mu_{\Sigma^-} &= \mu_{\Xi^-} = \mu_{\Delta^-} = \mu_n + \mu_e, \\
\mu_{\Delta^{++}} &= \mu_p - \mu_e, \\
\mu_{\Sigma^0} &= \mu_{\Xi^0} = \mu_{\Lambda^0} = \mu_{\Delta^0} = \mu_n.
\end{aligned} \tag{4.9}$$

In case of (anti)kaons, the threshold conditions are governed by the strangeness changing processes are discussed in sec.-3.2. The charge neutrality condition due to inclusion of (anti)kaons, heavier strange and non-strange particles along with leptons is modified as

$$\sum_b q_b n_b + \sum_\Delta q_\Delta n_\Delta - n_{K^-} - n_e - n_\mu = 0. \tag{4.10}$$

The total energy density due to the fermionic part is given by

$$\begin{aligned}\varepsilon_f = &\sum_{j\equiv b,\Delta} \frac{2J_j+1}{2\pi^2}\left[p_{F_j}E^3_{F_j} - \frac{m^{*2}_j}{8}\left(p_{F_j}E_{F_j} + m^{*2}_j \ln\left(\frac{p_{F_j}+E_{F_j}}{m^*_j}\right)\right)\right] \\ &+ \frac{1}{\pi^2}\sum_l \left[p_{F_l}E^3_{F_l} - \frac{m^2_l}{8}\left(p_{F_l}E_{F_l} + m^2_l \ln\left(\frac{p_{F_l}+E_{F_l}}{m_l}\right)\right)\right] \\ &+ \frac{1}{2}m^2_\sigma\sigma^2 + \frac{1}{2}m^2_\omega\omega^2_0 + \frac{1}{2}m^2_\rho\rho^2_{03} + \frac{1}{2}m^2_{\sigma^*}\sigma^{*2} + \frac{1}{2}m^2_\phi\phi^2_0.\end{aligned} \tag{4.11}$$

And the energy density contribution from the (anti)kaonic matter is

$$\varepsilon_{\bar{K}} = m^*_K(n_{K^-} + n_{\bar{K}^0}) \tag{4.12}$$

giving the total energy density as $\varepsilon = \varepsilon_{\bar{K}} + \varepsilon_f$. Now, because (anti)kaons being bosons are in the condensed phase at $T = 0$, the matter pressure is provided only by the baryons and leptons and is given by the Gibbs-Duhem relation

$$p_m = \sum_{j\equiv b,\Delta} \mu_j n_j + \sum_l \mu_l n_l - \varepsilon_f. \tag{4.13}$$

4.3 Coupling parameters

In the density dependent RMF model implemented in this work, DD-ME2 Lalazissis et al. [2005] coupling parametrization is incorporated. We have chosen this parametrization due to the reasons that, it reproduces the parameter estimations of nuclear symmetric as well as isospin asymmetric matter at nuclear saturation density which are in good agreement with recent experimental findings Gal et al. [2016]. The other reason is the capability to fulfil the massive $\sim 2\ M_\odot$ NS constraint. The coupling functional dependence of the scalar σ, vector ω and isovector-vector ρ-mesons on density are discussed in sec.-2.4. The parameters of the meson-nucleon couplings in DD-ME2 parametrization model is given in table-2.3. Since the nucleons do not couple to the strange mesons, $g_{\sigma^*N} = g_{\phi N} = 0$. The masses of the additional hidden strangeness mesons are taken as $m_{\sigma^*} = 975$ MeV and $m_\phi = 1019.45$ MeV. Table-4.1 provides the mass, electric charge and isospin of the different exotic particles considered in this work.

Table 4.1: Properties of the various exotic particles considered in this study.

Particles	Bare mass (MeV)	Charge (e)	Isospin
Λ	1115.68	0	0
Σ^+	1189.37	1	1
Σ^0	1192.64	0	0
Σ^-	1197.45	-1	-1
Ξ^0	1314.86	0	$1/2$
Ξ^-	1321.71	-1	$-1/2$
$K^-, \bar{K}^0$	493.69	$-1, 0$	$1/2, 1/2$
$\Delta^-, \Delta^0, \Delta^+, \Delta^{++}$	1232	$-1, 0, 1, 2$	$-3/2, -1/2, 1/2, 3/2$

4.3.1 Hyperon coupling constants

Due to inadequacy of reliable knowledge regarding the hyperon-nucleon as well as hyperon-hyperon interactions, the coupling estimations in this regard still remains an open question. For the meson-hyperon vector coupling parameters, we incorporated the SU(6) symmetry and quark counting rule following previous works of Schaffner et al. [1994] which provide

$$\begin{aligned}
&\frac{1}{2}g_{\omega\Lambda} = \frac{1}{2}g_{\omega\Sigma} = g_{\omega\Xi} = \frac{1}{3}g_{\omega N}, \\
&2g_{\phi\Lambda} = 2g_{\phi\Sigma} = g_{\phi\Xi} = -\frac{2\sqrt{2}}{3}g_{\omega N}, \\
&\frac{1}{2}g_{\rho\Sigma} = g_{\rho\Xi} = g_{\rho N}, \quad g_{\rho\Lambda} = 0.
\end{aligned} \tag{4.14}$$

The scalar meson-hyperon couplings can be calculated from the fits of their respective optical potentials in nuclear matter within a particular model. In this work, we have considered the optical potentials of Λ, Ξ, Σ in symmetric nuclear matter as

$$U_{\Lambda}^{(N)}(n_0) = -30 \text{ MeV}, \quad U_{\Xi}^{(N)}(n_0) = -14 \text{ MeV}, \quad U_{\Sigma}^{(N)}(n_0) = +30 \text{ MeV}, \tag{4.15}$$

at saturation density respectively following ref.-Li et al. [2018a]. The scalar hyperon-meson couplings considered in this study are compatible with the recent hypernuclei experiment findings as compiled in refs.-Feliciello and Nagae [2015]; Gal et al. [2016]. Recently ref.-Friedman and Gal [2021] reported an attractive optical potential depth of Ξ-hyperons in SNM to be $\gtrsim -20$ MeV. For a more recent review on the aspects of strangeness in dense matter, the reader may refer to Tolos and Fabbietti [2020]. The scalar strange meson σ^*–Λ coupling is evaluated from the measurements on light double-Λ nuclei and fitted to the optical potential depth $U_{\Lambda}^{\Lambda}(n_0/5) = -0.67$ MeV Li et al. [2018a] and further constraining the σ^*–Ξ and σ^*–Σ couplings via the relation

$$\frac{g_{\sigma^* Y}}{g_{\phi Y}} = \frac{g_{\sigma^*\Lambda}}{g_{\phi\Lambda}}, \quad Y \in \{\Xi, \Sigma\}. \tag{4.16}$$

Table-4.2 provides the numerical values of the meson-hyperon couplings at nuclear saturation density, where $R_{\sigma Y} = g_{\sigma Y}/g_{\sigma N}$, $R_{\sigma^* Y} = g_{\sigma^* Y}/g_{\sigma N}$ denote the scaling factors for non-strange and strange scalar mesons coupling to hyperons respectively.

Table 4.2: Scalar meson-hyperon coupling constants for DD-ME2 parametrization.

	Λ	Ξ	Σ
$R_{\sigma Y}$	0.6105	0.3024	0.4426
$R_{\sigma^* Y}$	0.4777	0.9554	0.4777

4.3.2 Δ-resonances coupling constants

Because experimental information on the Δ-resonance is scarce, the meson-Δ baryon couplings are treated as parameters. Refs.-Nakamura et al. [2010]; Koch and Ohtsuka [1985]; Wehrberger et al. [1989] have reported the data to constrain meson-Δ baryon couplings at n_0

based on pion-nucleus scattering, electron scattering on nuclei and excitation studies of Δ-quartet experiments. Recent studies [Drago et al., 2014; Klähn et al., 2006; Kolomeitsev et al., 2017] on this aspect have reported the Δ-potential (V_Δ) in nuclear medium to be in the range

$$-30 \text{ MeV} + V_N(n_0) \leq V_\Delta(n_0) \leq V_N(n_0), \tag{4.17}$$

with $V_N(n_0)$ being the nucleon potential at saturation density and the values of factor $R_{\sigma\Delta} - R_{\omega\Delta}$ to be between 0 and 0.2 with $R_{\sigma\Delta} = g_{\sigma\Delta}/g_{\sigma N}$ and $R_{\omega\Delta} = g_{\omega\Delta}/g_{\omega N}$. Many works Drago et al. [2014]; Kolomeitsev et al. [2017]; Li et al. [2018b]; Ribes et al. [2019]; Chen et al. [2007]; Cai et al. [2015]; Raduta [2021] have considered the ranges for $R_{\omega\Delta} \in [0.6 - 1.2]$ and $R_{\rho\Delta} \in [0.5 - 3.0]$. For recent development regarding Δ-potential in dense matter, the reader may refer to Cozma and Tsang [2021]. In the subsequent discussion we consider $R_{\omega\Delta} = 1.10$ and $R_{\rho\Delta} = 1.00$ for vector-meson couplings. For the scalar meson-Δ baryon couplings we use two values of $R_{\sigma\Delta} = 1.10,\ 1.23$ corresponding to $V_\Delta = V_N$ and $5/3\ V_N$ respectively. Similar to the nucleons, Δ-resonances do not couple to σ^*, ϕ-mesons, i.e, $R_{\sigma^*\Delta} = R_{\phi\Delta} = 0$.

4.3.3 (Anti)kaon coupling constants

The meson-(anti)kaon couplings are considered as density-independent. The vector meson-(anti)kaon coupling parameters are adapted similarly as discussed in sec.-3.3. For the scalar meson-(anti)kaon coupling constants, we calculate by fitting to the real part of K^- optical potential at n_0. We have chosen a K^- optical potential range of $-120 \leq U_{\bar{K}} \leq -150$ MeV in this work and numerical values of $g_{\sigma K}$ for the mentioned optical potential range is provided in table-4.3.

Table 4.3: Scalar σ meson-(anti)kaon coupling parameter values in DD-ME2 parametrization at n_0.

$U_{\bar{K}}$ (MeV)	−120	−130	−140	−150
$g_{\sigma K}$	0.4311	0.6932	0.9553	1.2175

Since, the (anti)kaons possess strange quarks, so the (anti)kaons will interact via the mediation of the additional hidden strange force mediating mesons. The scalar σ^*-meson coupling to (anti)kaon is estimated from the decay of $f_0(925)$ as $g_{\sigma^* K} = 2.65$ and that for the vector ϕ-meson coupling is obtained from the SU(3) relation of the quark model as $g_{\phi K} = 4.27$ [Schaffner and Mishustin, 1996].

4.4 Results and discussion

In this section, we report our numerical results for matter composition with (anti)kaons and (a) Nucleons + Hyperons (NY), (b) Nucleons + Hyperons + Δ-resonances (NYΔ) for varying values of (anti)kaon optical potentials. The case of pure nuclear matter with (anti)kaons is already discussed in chapter-3. From calculations, it is found that the phase transition to (anti)kaon condensed phase is of the second-order for both NY and NYΔ compositions. In all the calculations the K^--meson is observed to appear before the onset of $\bar{K}^0$.

Table-4.4 provides the threshold densities of (anti)kaons for different values of Δ-baryon as well as $U_{\bar{K}}$ potentials for three matter compositions, viz. N, NY and NYΔ. As already

Table 4.4: Threshold densities, n_u for (anti)kaon condensation in N, NY and NYΔ matter for different values of Δ-potentials and K^- optical potential depths $U_{\bar{K}}(n_0)$.

Config. $\rightarrow$	N$\bar{K}$		NY$\bar{K}$		NY$\Delta\bar{K}$			
					$R_{\sigma\Delta} = 1.10$		$R_{\sigma\Delta} = 1.23$	
$U_{\bar{K}}$ $\downarrow$ (MeV)	$n_u(K^-)$ (n_0)	$n_u(\bar{K}^0)$ (n_0)	$n_u(K^-)$ (n_0)	$n_u(\bar{K}^0)$ (n_0)	$n_u(K^-)$ (n_0)	$n_u(\bar{K}^0)$ (n_0)	$n_u(K^-)$ (n_0)	$n_u(\bar{K}^0)$ (n_0)
-120	3.00	4.89	–	–	–	–	–	–
-130	2.85	4.65	–	–	–	–	5.86	6.79
-140	2.72	4.42	3.97	6.95	4.26	6.92	4.37	5.05
-150	2.59	4.19	3.06	5.59	3.33	5.39	3.90	4.37

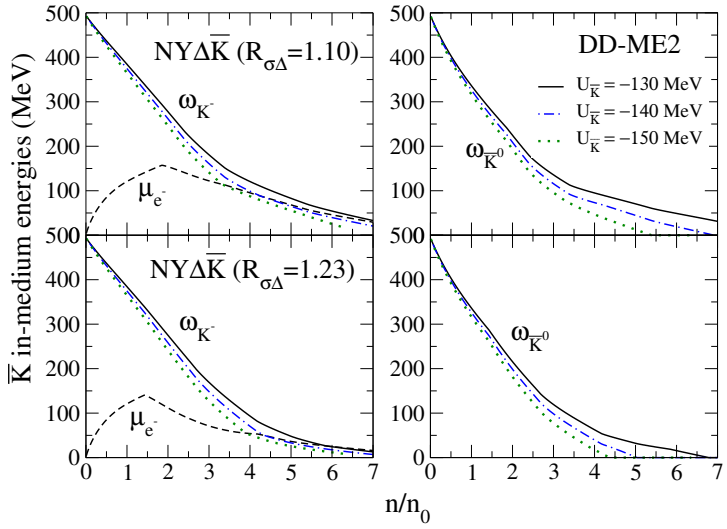

Figure 4.1: The effective energy of (anti)kaons as a function of baryon number density in NYΔ matter for Δ-potential values $R_{\sigma\Delta} = 1.10$ (top panels) and $R_{\sigma\Delta} = 1.23$ (bottom panels). Left and right panels show the energies of K^- and $\bar{K}^0$ respectively. The chemical potential of electron for the same matter composition is depicted by the dashed curve. The solid, dash-dotted, dotted lines represent the $U_{\bar{K}}$ values of $-130, -140, -150$ MeV respectively.

discussed in chapter-3, the (anti)kaons in nucleonic matter appears as early as $\sim 2.6\ n_0$ with $U_{\bar{K}} = -150$ MeV. The onset of hyperons pushes the threshold densities of (anti)kaons to higher densities in comparison to cases with only nucleonic matter. It is observed that the (anti)kaons do not appear at all in case of $U_{\bar{K}} = -120$ MeV for NY and NYΔ matter compositions. (Anti)kaons are observed to appear only after $U_{\bar{K}} = -130$ MeV with $R_{\sigma\Delta} = 1.23$. This happens as the higher Δ-potential shifts the onset of hyperons to higher densities making the way for the (anti)kaons. In all the cases considered, it is observed that with the inclusion of Δ-resonances into the composition of matter the threshold densities of onset of (anti)kaon is shifted to higher densities.

Fig.-4.1 shows the in-medium (effective) energies of $\bar{K}$ mesons as a function of baryon (vector) number density in NYΔ matter described by the DD-ME2 coupling model. With the increase in the values of $U_{\bar{K}}$, the density threshold for the onset of the (anti)kaons is shifted to

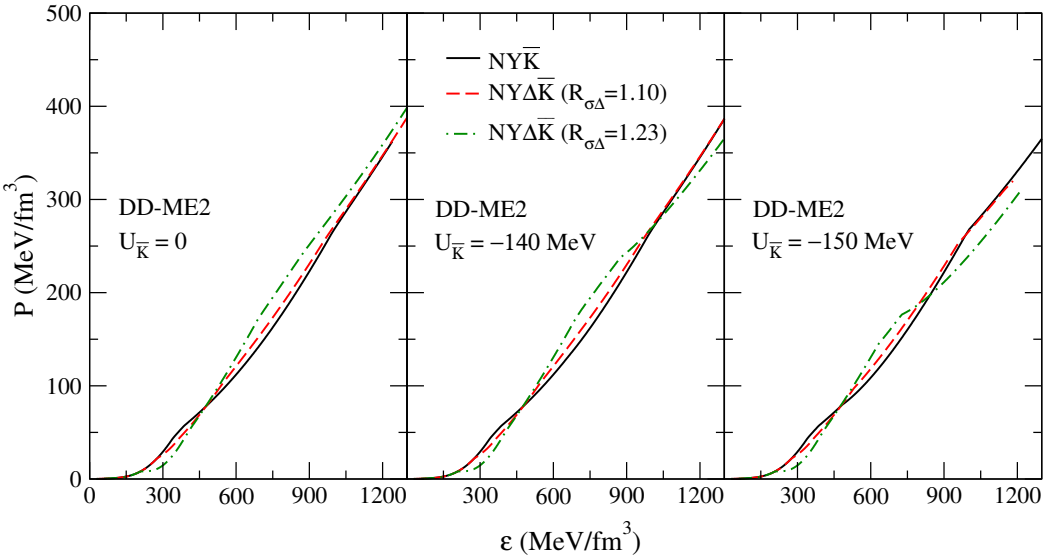

Figure 4.2: Pressure as a function of energy density (EoS) for zero-temperature, charge-neutral NY matter (solid lines), NYΔ matter with Δ-potential $R_{\sigma\Delta} = 1.10$ (dashed lines) and $R_{\sigma\Delta} = 1.23$ (dash-dotted lines). The three panels correspond to different values of (anti)kaon potential: $U_{\bar{K}} = 0$ (left panel), $U_{\bar{K}} = -140$ (middle panel), and $U_{\bar{K}} = -150$ MeV (right panel).

lower densities.

The EoSs with NY and NYΔ matter compositions in the absence as well as in presence of (anti)kaon degrees of freedom are shown in fig.-4.2. When compared for the cases with (anti)kaons in N (please refer to left panel of fig.-3.9) and NY matter as in middle and right panels of fig.-4.2, it may be observed that the role of (anti)kaons in softening of dense matter EoS for the latter case is significantly less in comparison to the former one. This is due to the same reason that hyperon threshold densities are earlier than (anti)kaon ones. In the case with no (anti)kaons in matter, the EoSs of NYΔ matter is stiffer than the EoS of NY matter in the high-density regime and the opposite is true in the low-density regime. The middle and right panels of fig.-4.2 include (anti)kaons with potential values $U_{\bar{K}} = -140, -150$ MeV respectively. It is seen that the onset of (anti)kaon condensation softens the EoS, which is marked by a change in the slope of EoSs beyond the condensation threshold. Furthermore, the softening is more pronounced in the case of NYΔ composition, which reverses the high-density behavior seen in the left panel: the EoS with NYΔ composition is now the softest among all considered cases. It is further seen that the higher the value of $U_{\bar{K}}$ the more pronounced is the softening of the EoSs. This is because of the fact that higher $U_{\bar{K}}$ favours larger presence of (anti)kaons which softens the dense matter EoSs.

The mass-radius (M-R) relations corresponding to the EoSs in fig.-4.2 were obtained by solving the TOV equations for static non-rotating spherical stars and are shown in fig.-4.3. For the crust region, the Baym, Pethick and Sutherland (BPS) [Baym et al., 1971b] and Baym, Bethe, Pethick (BBP) [Baym et al., 1971a] EoSs are implemented following thermodynamic consistency. The inclusion of additional exotic degrees of freedom reduces the maximum mass of NSs in comparison to nucleonic matter from 2.5 $M_\odot$ to ~ 2 $M_\odot$. Following the comparison of EoSs with (anti)kaons in N and NY matter as in previous paragraph, the TOV solutions for

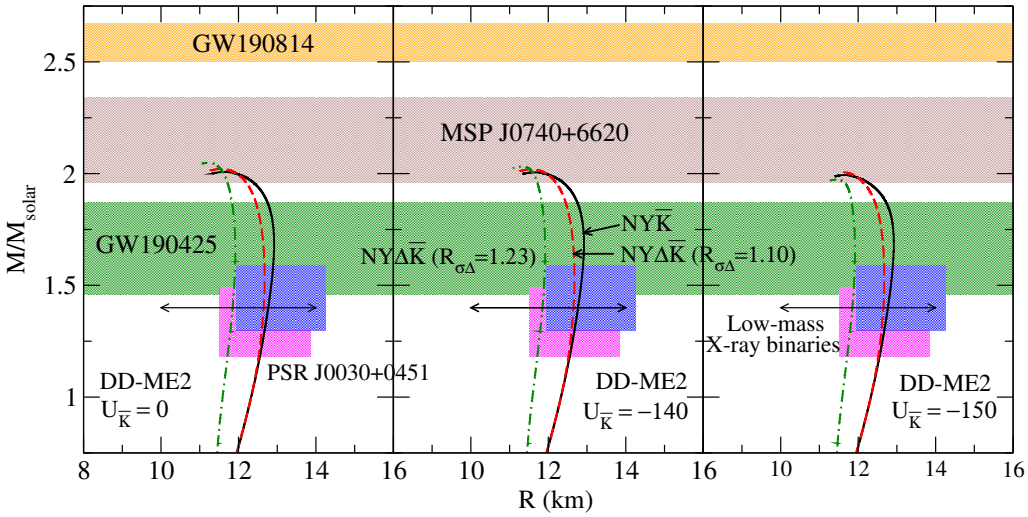

Figure 4.3: The mass-radius relationships for EoS shown in fig.-4.2 for NY matter (solid lines), NYΔ matter with Δ-potential $R_{\sigma\Delta} = 1.10$ (dashed lines) and $R_{\sigma\Delta} = 1.23$ (dash-dotted lines). The three panels correspond to different values of (anti)kaon potential: $U_{\bar{K}} = 0$, i.e., no (anti)kaon condensation, (left panel), $U_{\bar{K}} = -140$ (middle panel), and $U_{\bar{K}} = -150$ MeV (right panel). The astrophysical constraints from GW190425 [Abbott et al., 2020a], GW190814 [Abbott et al., 2020b], MSP J0740+6620 [Cromartie et al., 2020], PSR J0030+0451 [Miller et al., 2019; Riley et al., 2019], low-mass X-ray binaries [Steiner et al., 2018] are marked by the shaded regions.

the same can be seen in fig.-3.10 and 4.3. The lowering of maximum mass configuration considering similar optical potential of (anti)kaons in dense matter is a clear evident of EoS softening due to inclusion of strange baryons. The compactness is also observed to be enhanced due to the appearance of Δ^--resonance at lower densities. The parameter values of the maximum mass stars are provided in a tabulated form in table-4.5. From tables-4.4 and 4.5 it can be inferred that K^- meson appears in all the EoS models with $U_{\bar{K}} = -140, -150$ MeV. But $\bar{K}^0$ meson does not appear in the hypernuclear star with $U_{\bar{K}} = -140$ MeV and Δ-baryon admixed hypernuclear star with $R_{\sigma\Delta} = 1.10$ and $U_{\bar{K}} = -140$ MeV. Consistent with the (anti)kaon softening of the EoS seen in fig.-4.2 the maximum masses of the stars with NYΔ composition and (anti)kaon condensation lie below those without Δ resonances, which is the reverse of what is observed when (anti)kaon condensation is absent.

From the analysis above, we conclude that compact stars containing (anti)kaons are consistent with the astrophysical constraints set by the observations of massive pulsars, the NICER measurements of parameters of PSR J0030 + 0451, the low-mass X-ray binaries in a globular cluster, and the gravitational wave event GW190425. Although we do not provide here the deformabilities of our models, from the values of the radii obtained it is clear that our models are also consistent with the GW170817 event. Finally, our models are inconsistent with the interpretation of the light companion of the GW190814 binary as a compact star. Including the rotation even at its maximal mass-shedding limit will not be sufficient to produce a $\sim 2.5 M_\odot$ mass compact star, the readers can refer to refs.-Sedrakian et al. [2020]; Li et al. [2020].

Fig.-4.4 shows the particle composition in NY matter with (anti)kaons as a function of baryon number density and for $U_{\bar{K}} = -140, -150$ MeV. At low densities, before the onset of

Table 4.5: Properties of maximum mass stars for various compositions and values of (anti)kaon potential $U_{\bar{K}}(n_0)$. For each composition/potential value the enteries include: maximum mass (in units of $M_\odot$) the radius, and central number density.

Configuration →	NY$\bar{K}$			NY$\Delta\bar{K}$					
				$R_{\sigma\Delta}=1.10$			$R_{\sigma\Delta}=1.23$		
$U_{\bar{K}}$ ↓ (MeV)	$M_{\max}$ ($M_\odot$)	R (km)	n_c (n_0)	$M_{\max}$ ($M_\odot$)	R (km)	n_c (n_0)	$M_{\max}$ ($M_\odot$)	R (km)	n_c (n_0)
0	2.008	11.651	6.107	2.021	11.565	6.160	2.049	11.226	6.349
−140	2.005	11.652	6.096	2.019	11.566	6.151	2.032	11.343	6.214
−150	1.994	11.664	6.13	2.006	11.61	6.143	1.973	11.448	6.028

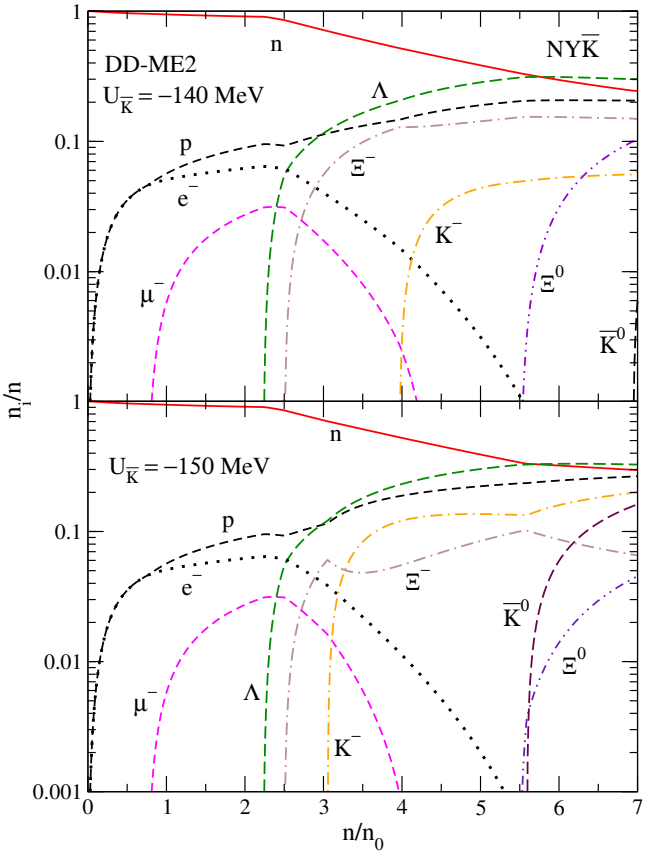

Figure 4.4: Particle abundances n_i (in units of n) as a function of normalized baryon number density in NY matter for values of $U_{\bar{K}} - 140$ MeV (top panel) and -150 MeV (bottom panel).

strange particles, the charge neutrality is maintained among the protons, electrons and muons. At somewhat higher density ($\geq 2n_0$) Λ and Ξ^- appear (because of the repulsive nature of Σ-potential in dense nuclear matter, Σ-baryons do not appear in the composition). Finally, the (anti) kaons and Ξ^0 appear in the high-density regime ($\geq 4n_0$). Comparing the upper and lower panels of the figure, we observe that the higher $|U_{\bar{K}}|$ value implies a lower density threshold of the onset of (anti)kaon, as expected. The onset of (anti)kaons also affects the population of leptons; K^- are efficient in replacing electrons and muons once they appear,

thus they contribute to the extinction of leptons, which occurs at lower densities for higher values of $|U_{\bar{K}}|$. In the case of $U_{\bar{K}} = -150$ MeV, the Ξ^- fraction is seen to be strongly affected by the appearance of K^- mesons. This is expected as K^- being bosons are more energetically favorable for maintaining the charge neutrality compared to fermionic Ξ^-. The composition in the case of $U_{\bar{K}} = -140$ MeV, does have $\bar{K}^0$ mesons ($n_u \sim 6.95\ n_0$) whereas for $U_{\bar{K}} = -150$ MeV, $\bar{K}^0$ appears at onset density $n_u \sim 5.59\ n_0$ which leads to an additional softening of the EoS.

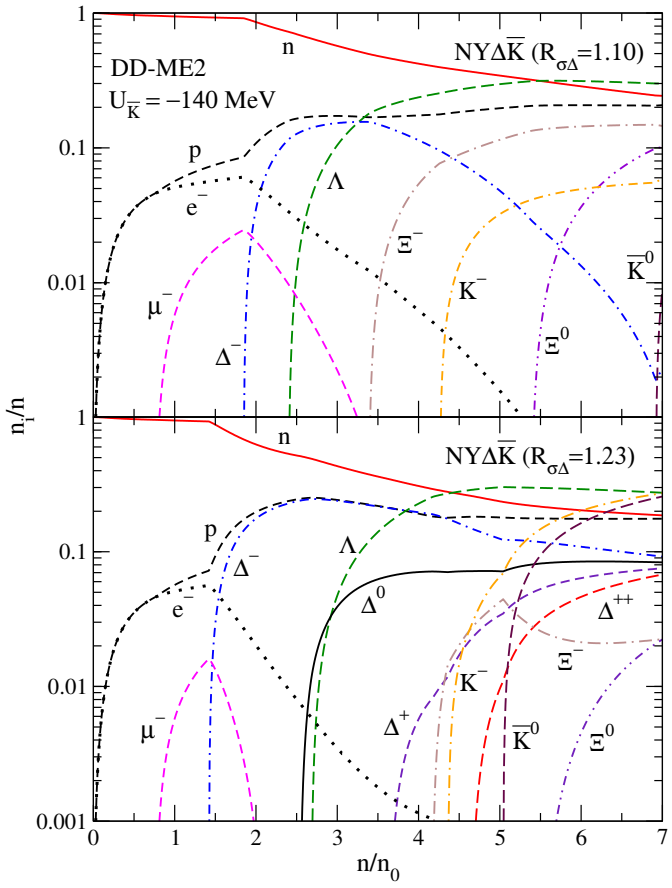

Figure 4.5: Same as fig.-4.4 but for NYΔ matter for $R_{\sigma\Delta} = 1.10$ (top panel) and $R_{\sigma\Delta} = 1.23$ (bottom panel) and fixed value of $U_{\bar{K}} = -140$ MeV.

Fig.-4.5, which is analogous to fig. 4.4, shows the particle population in $NY\Delta$-matter as a function of baryon number density for $U_{\bar{K}} = -140$ MeV. It is observed that for $R_{\sigma\Delta} = 1.10$ only Δ^- resonance appears, whereas for $R_{\sigma\Delta} = 1.23$ the onset of the entire quartet of Δ-resonances is possible. It seen that in general the Δ-resonances effectively shift the threshold densities of hyperons to higher densities, thus diminishing their role. This concerns both the neutral Λ as well as Ξ^--hyperon. This shift is stronger for larger values of $R_{\sigma\Delta}$. Resonances also suppress the lepton fraction by lowering the density at which they disappear in NYΔ-matter, this effect being magnified for larger values of V_Δ. In the high-density regime the negative charge is provided by Δ^-–Ξ^-–K^- mixture and it is seen that the rapid increase in the K^- population suppresses the Δ^--Ξ^- abundances for $R_{\sigma\Delta} = 1.23$, as kaons are energetically more favorable than the heavy-baryons. Note also that the onset of $\bar{K}^0$ meson abruptly decreases the abundance of Ξ^-, as seen in the lower panel; (in the upper panel, i.e. for $U_{\bar{K}} = -140$ MeV and $R_{\sigma\Delta} = 1.10$, the $\bar{K}^0$ mesons do not appear). There is some qualitative differences between

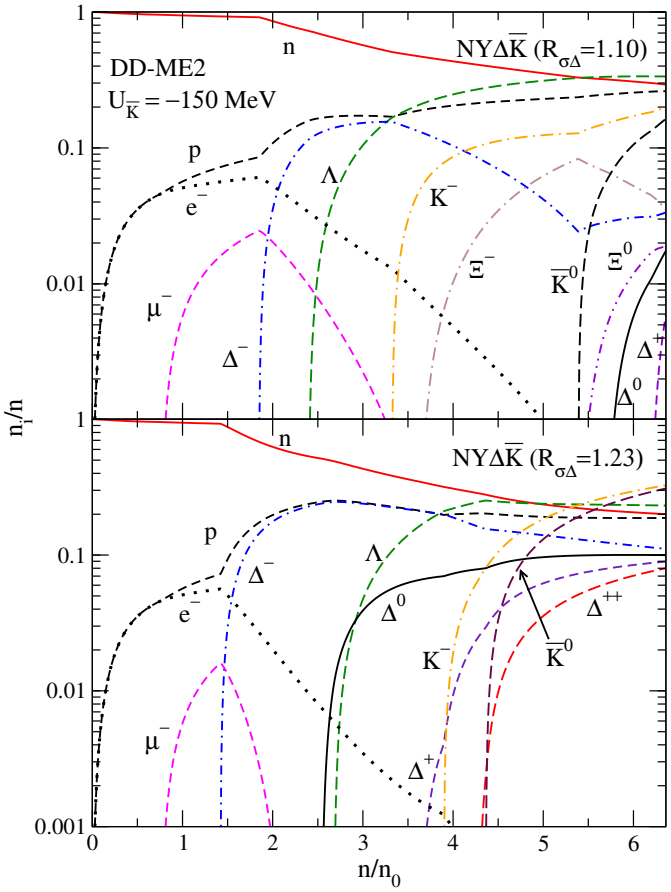

Figure 4.6: Same as fig.-4.5 but for a larger (absolute) value of potential $U_{\bar{K}} = -150$ MeV.

the two cases $R_{\sigma\Delta} = 1.10$ and 1.23: (a) the Δ^- baryon disappears at higher matter densities for $R_{\sigma\Delta} = 1.10$ but its abundance is almost constant in for $R_{\sigma\Delta} = 1.23$; (b) the Λ hyperon dominates over the neutron fraction at higher density for $\sim 5.5\ n_0$ in case of $R_{\sigma\Delta} = 1.10$ compared to $\sim 4.5\ n_0$ in case of $R_{\sigma\Delta} = 1.23$.

Fig.-4.6 shows the same as in fig.-4.5 but for $U_{\bar{K}} = -150$ MeV. The particle fractions show identical trends as in fig.-4.5 until the appearance of (anti)kaons. The larger potential favors earlier onset of (anti)kaons in matter; for example, the K^- sets in before the Ξ^- and it is now the dominant negatively charged component shortly after the density increases beyond the onset value. The effect of the onset of $\bar{K}^0$ on the Ξ^- and Δ^-, which is mediated via changes in the abundances of K^-, is seen clearly again. As before, for a large value of $R_{\sigma\Delta} = 1.23$, all the members of the quartet of Δ-resonances are present in the matter composition. Another notable fact is the complete extinction of $\Xi^{-,0}$ baryons, which is consistent with the trends seen in figs.-4.4 and 4.5. Interestingly, in the case $R_{\sigma\Delta} = 1.23$ the (anti)kaons abundances are the largest among all particles in the high-density regime, which leads also to the softening of the EoS observed above.

Fig.-4.7 shows the (anti)kaon effective mass as a function of normalized baryon number density for various strengths of $U_{\bar{K}}$ with different matter compositions. The effective mass of (anti)kaons tends to decrease rather steeply in case of higher strengths of $U_{\bar{K}}$. It is observed

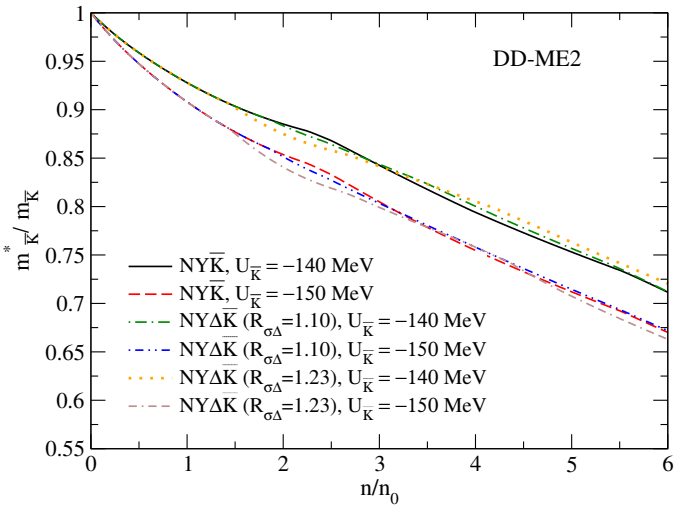

Figure 4.7: Effective (anti)kaon mass (in units of its bare mass, $m_{\bar{K}}$) as a function of baryon number density for NY and NYΔ matter compositions and two values of (anti)kaon potential depth.

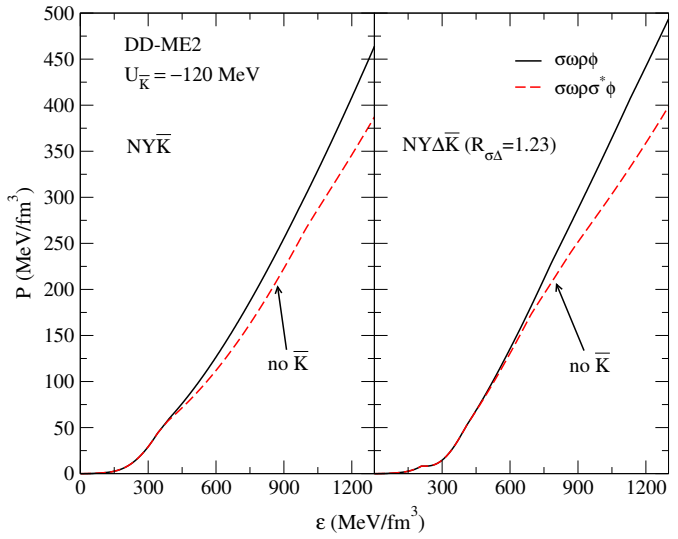

Figure 4.8: The EoS of NY matter (left panel) and NYΔ matter (right panel) with (anti)kaon potential $U_{\bar{K}} = -120$ MeV including σ^* meson (dashed lines) and without it (solid lines). The Δ-potential value is fixed at $R_{\sigma\Delta} = 1.23$.

that in the low-density regime, the (anti)kaon effective mass decreases relatively quickly in the case of Δ-resonances admixed matter compared to that with the only hyperonic matter. The reason is the larger scalar potential values arising from the onset of additional non-strange baryons at lower densities. And at higher densities, the (anti)kaon effective mass values are observed to be larger in the former case than the latter one. This may be attributed to the delayed onset of hyperons because of the Δ-resonances appearance.

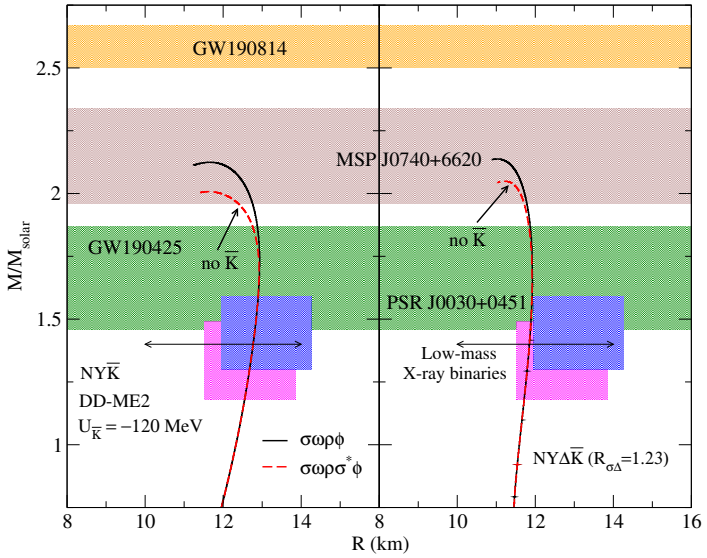

Figure 4.9: The M-R relations corresponding to the EoSs in fig.-4.8 are shown for NY matter (left panel) and NYΔ matter (right panel) with (anti)kaon potential $U_{\bar{K}} = -120$ MeV including σ^* meson (dashed lines) and without it (solid lines). The Δ-potential value is fixed at $R_{\sigma\Delta} = 1.23$. The astrophysical observables (constraints) are similar as in fig.-4.3.

The matter pressure as a function of energy density for different matter compositions with and without σ^* meson for the hyperon-hyperon interactions is shown in fig.-4.8. Being a scalar, σ^* meson makes the EoS softer as is evident from the figure. It is observed that incorporating σ^* meson rules out the possibility of (anti)kaon phase transition with $U_{\bar{K}} = -120$ MeV. This is because in the case with σ^*-meson, the difference of chemical potential of neutron and proton approaches zero as we go higher in density which eradicates the possibility of (anti)kaons appearance (refer to fig.-4.10). The phase transition from the purely hadronic to (anti)kaon condensed phase is second-order.

The results of mass-radius (M-R) relationship obtained by solving the TOV equations for non-rotating spherical stars corresponding to the EoSs in fig.-4.8 are presented in fig.-4.9. It is observed that in both cases of NY for NYΔ matter the inclusion of σ^* meson leads to lower maximum mass. It is also seen that the addition of Δ's reduces the radius of the of the stars and mildly increases the maximum mass, which consistent with the findings without (anti)kaon condensation. Table-4.6 provides the stellar maximum masses, radii and corresponding central densities evaluated from the EoSs in fig.-4.8 with $U_{\bar{K}} = -120$ MeV.

Table 4.6: Properties of maximum mass stars for various compositions, $U_{\bar{K}} = -120$ MeV, $R_{\sigma\Delta} = 1.23$ in the cases with σ^* meson and without. In both cases we list the maximum mass, the radius and central number density.

Config.	NY$\bar{K}$			NY$\Delta\bar{K}$ ($R_{\sigma\Delta} = 1.23$)		
	$M_{\rm max}$ ($M_\odot$)	R (km)	n_c (n_0)	$M_{\rm max}$ ($M_\odot$)	R (km)	n_c (n_0)
$\sigma\omega\rho\phi$	2.124	11.673	5.973	2.137	11.023	6.538
$\sigma\omega\rho\sigma^*\phi$	2.008	11.651	6.107	2.049	11.226	6.349

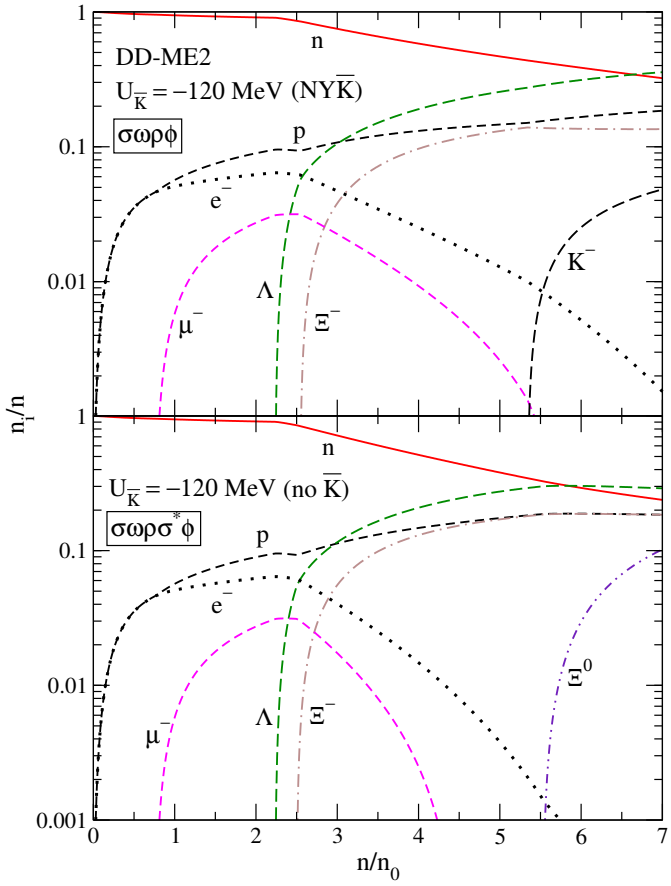

Figure 4.10: Particle abundances n_i (in units of n) as a function of normalized baryon number density in NY matter for value of $U_{\bar{K}} = -120$ in the case of $\sigma\omega\rho\phi$ exchange (top panel) and $\sigma\omega\rho\sigma^*\phi$ (bottom panel). (Anti)kaons are absent in the second case.

Fig.-4.10 shows the particle abundances in case of hypernuclear matter with $U_{\bar{K}} = -120$ MeV with and without σ^* meson. The main qualitative difference is that K^- appears for $n \geq 5.4\ n_0$ in the first case and it does not appear up to $n \sim 7\ n_0$ in the second case. Consequently, the charge neutrality is maintained between $e - \Xi^- + K^-$ and protons in the first case and only $e - \Xi^-$ and protons in the second case. Given by more than one order of magnitude smaller abundance of electrons, the abundances of Ξ^- and protons almost coincide in the second case. Another feature seen in fig.-4.10 is that the electron and muon populations disappear faster with increasing density in the case where the σ^* meson is included.

Fig.-4.11, which is similar to fig.-4.10, shows the composition of particles in NYΔ matter and for $U_{\bar{K}} = -120$ MeV. In this case also, (anti)kaons are observed to appear only in the EoS where σ^* meson is excluded. It is seen, that the main difference between the two cases is that σ^* driven interactions prefer lower threshold density of Ξ^0 and their larger fraction, which effectively leads to an exclusion of (anti)kaons in the density range considered. Unlike the case with only hypernuclear matter, in this case the lepton fractions are unaffected by the exclusion or inclusion of σ^* meson, because of the negative charge is supplied by the Δ^--resonance.

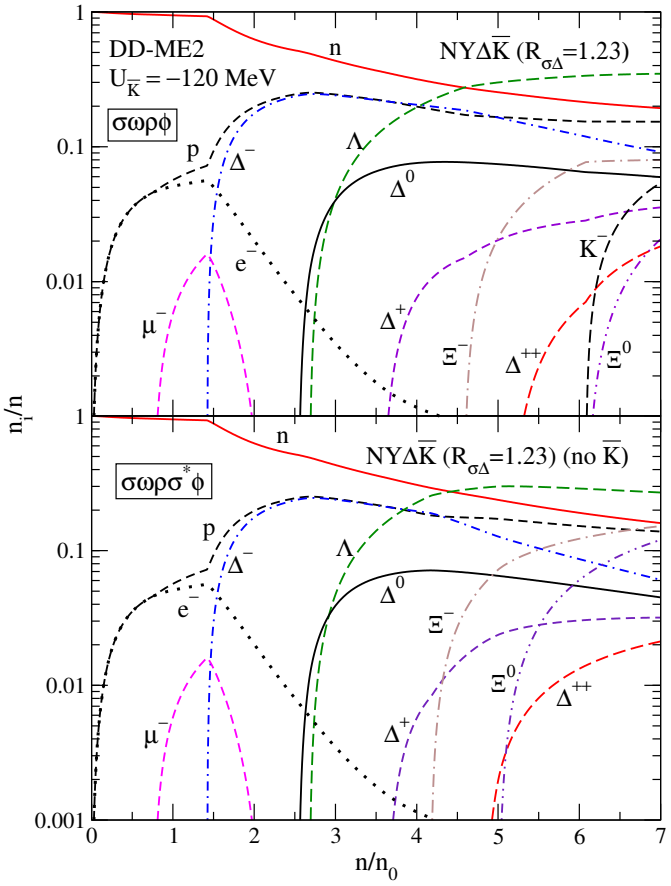

Figure 4.11: Same as fig.-4.10 but for NYΔ matter with $R_{\sigma\Delta} = 1.23$.

4.5 Summary

In this chapter, we discussed the second-order phase transition to Bose-Einstein condensation of (anti)kaons in hypernuclear matter with and without an admixture of Δ-resonances within the framework of density-dependent RMF theory. The resulting EoS, matter composition, and the structure of the associated static, spherically symmetrical star models were presented. The strong interactions viz. baryon-baryon and (anti)kaon-baryon are handled on the same footing. The K^- optical potentials ($-120 \leq U_{\bar{K}} \leq -150$ MeV) at nuclear saturation density are considered in a range which fulfills the observational compact star maximum mass constraint ($\sim 2M_{\odot}$).

We find that the (anti)kaon condensates cannot appear in the hypernuclear matter, within our parametrization, if $U_{\bar{K}} \leq -130$ MeV. $\bar{K}^0$ condensation is absent in maximum mass compact stars with $U_{\bar{K}} = -140$ MeV. The inclusion of hyperons into the matter composition shifts the onset of (anti)kaons to higher density regimes in comparison to the case without hyperons, i.e. only nuclear matter, c.f. to chapter-3. For higher $U_{\bar{K}}$ values, the appearance of both the (anti)kaons becomes possible in the maximum mass models. The K^- meson fraction is seen to dominate over the Ξ^- baryon for high $U_{\bar{K}}$ strengths. This can be attributed to the fact that the K^- particle being bosons is more favored over the fermionic Ξ^--particles.

Next, in the case of Δ baryon admixed hypernuclear matter, the onset of (anti)kaons is shifted to even higher densities compared to only hyperonic matter. (Anti)kaon condensation is absent with $U_{\bar{K}} \leq -120$ MeV. The condensed phase is observed to appear in matter with $U_{\bar{K}} = -130$ MeV and $R_{\sigma\Delta} = 1.10$. However, $\bar{K}^0$ condensation is absent for this particular $U_{\bar{K}}$ strength. Larger values of Δ-potentials $R_{\sigma\Delta}$ imply that the entire Δ-resonances quartet is present in matter. It is also observed that in a particular matter composition ($U_{\bar{K}} = -150$ MeV, $R_{\sigma\Delta} = 1.10$), the onset of K^- occurs even before that of Ξ^- particles. Moreover, for higher strengths of $U_{\bar{K}}$ and $R_{\sigma\Delta}$, the Δ-baryons and (anti)kaons take over the $\Xi^{-,0}$ particles leading to their complete suppression in the matter. Lepton populations are suppressed with increasing density more quickly in case of higher strengths of $R_{\sigma\Delta}$. We find that the effective mass of (anti)kaons is weakly dependent on the composition of matter and decreases almost linearly in the relevant density range $2 \leq n/n_0 \leq 6$, which reflects the density dependence of the scalar potential.

The influence of the strange scalar interaction mediating meson σ^* on the composition and EoS are twofold: firstly, including the σ^* meson softens the EoS significantly leading to lower maximum masses of compact stars. Secondly, exclusion of σ^* meson allows for (anti)kaon K^- to appear for weakly attractive potential strength $U_{\bar{K}} \sim -120$ MeV in both the hyperonic as well as Δ admix hypernuclear matter.

As indicated in the discussion (sec.-4.4), the present model with a suitable choice of parameters characterizing the (anti)kaon condensate is consistent with the currently available astrophysical constraints. The present model can, therefore, be used to model physical processes in (anti)kaon condensate featuring Δ-admixed hypernuclear star. Examples include cooling processes, bulk viscosity, thermal conductivity, to list a few.